

# Beyond Localization: A Comprehensive Diagnosis of Perspective-Conditioned Spatial Reasoning in MLLMs from Omnidirectional Images

Yuangong Chen<sup>1</sup>, Wai Keung Wong<sup>1,†</sup>, Jiaxing Li<sup>2</sup>,  
Ioannis Patras<sup>3</sup>, Xu Zheng<sup>3,4</sup>

<sup>1</sup>The Hong Kong Polytechnic University <sup>2</sup>Guangzhou University <sup>3</sup>Queen Mary University of London  
<sup>4</sup>HKUST(Guangzhou)

caleb.chen@connect.polyu.hk; {calvin.wong, jiaxing.li}@polyu.edu.hk; i.patras@eecs.qmul.ac.uk; zhengxu128@gmail.com

**Foundational Perception Tasks (T0-T2):** verify whether models can reliably extract spatial primitives—such as occluded counts, proximity, and allocentric directions—directly from the default 360° observation

<b>T0: Object Counting</b> <b>Q:</b> How many table(s) are there in this scene? <b>A:</b> 2	<b>T1: Relative Distance</b> <b>Q:</b> Which of these objects ( <i>chair, tv, table, fridge</i> ) is the <b>closest to</b> the <i>trash_can</i> ? <b>A:</b> <i>fridge</i>	<b>T2: Relative Direction</b> <b>Q:</b> Where is <i>fridge</i> <b>relative to</b> <i>trash_can</i> ? <b>A:</b> <i>left</i>
<b>Premise:</b> <i>Sofa</i> is left of <i>table</i> ; <i>Table</i> is left of <i>cabinet</i> . <b>Q:</b> <b>Position of <i>sofa</i> relative to <i>cabinet</i>?</b> <b>A:</b> <i>Left</i>	<b>Premise:</b> Stand at <i>cabinet</i> , face <i>table</i> , then <b>rotate 90° clockwise</b> . <b>Q:</b> What is now <b>at the center</b> ? <b>A:</b> <i>trash_can</i>	<b>Premise:</b> If stand at <i>cabinet</i> , face <i>table</i> , FoV narrows. <b>Q:</b> <b>Can you see</b> the couch? <b>A:</b> <i>Yes</i>
<b>T3: Compositional Chains</b>	<b>T4: Egocentric Rotation</b>	<b>T7: Limited-FOV Visibility</b>

**Advanced PCSR Tasks (T3-T7):** demanding mental simulation within the model's internal representation

**Figure 1: Diagnostic task structure of PCSR-Bench and examples, with foundational perception tasks (T0–T2, upper part) and advanced perspective-conditioned spatial reasoning (PCSR) tasks (T3–T7, lower part).**

## Abstract

Multimodal Large Language Models (MLLMs) show strong visual perception, yet remain limited in reasoning about space under changing viewpoints. We study this challenge as **Perspective-Conditioned Spatial Reasoning (PCSR)** in 360° omnidirectional images, where broad scene coverage reduces ambiguity from partial observations without eliminating the need for viewpoint-dependent inference. To assess this capability, we introduce **PCSR-Bench**, a diagnostic benchmark of 84,373 question–answer pairs from 2,600 omnidirectional images across 26 indoor environments. PCSR-Bench contains eight tasks spanning foundational perception (e.g., object counting, relative distance, and relative direction) and **advanced PCSR**, including compositional chains, egocentric rotation, perspective re-anchoring, ego-distortion, and limited-FOV visibility. We evaluate 14 representative MLLMs and observe a substantial

perception–reasoning gap: accuracy reaches 57.59% on foundational relative direction, but drops to 13.49% on egocentric rotation, 7.13% on egocentric distortion, and 0.64% on open-ended compositional reasoning. To probe the plasticity of this gap, we conduct an RL-based diagnostic study on a 7B-scale model. Reward shaping improves a matched 7B baseline from 31.10% to 60.06% under a controlled setting, suggesting that PCSR is partial plasticity rather than being fully immutable. Still, the gains are task-selective, sensitive to reward design including both weight allocation and reward formulation, and partially dependent on the evaluation protocol. These results position PCSR as a key bottleneck in current MLLMs and highlight limited but meaningful room for recovery under targeted optimization.

## CCS Concepts

• **Computing methodologies** → **Spatial and physical reasoning**; **Scene understanding**; *Natural language processing*; Scene analysis.

## Keywords

MLLMs, Perspective-Conditioned Spatial Reasoning, Omnidirectional Images, Reinforcement Learning (RL)

## 1 Introduction

A seemingly simple request—“Take the plate on the right side of the table to the kitchen”—requires an agent not only to locate the table and the plate, but also to interpret the spatial relation *right side* with respect to the speaker’s position and viewpoint. As the observer moves or turns, relations such as left/right, front/back, and even visibility may change accordingly. This reflects a fundamental property of spatial cognition: viewpoint change requires more than static object recognition, and has long been studied as a problem of mental transformation and internal spatial modeling [15, 29, 37, 44]. Recent evidence further suggests that current vision-language models exhibit a persistent egocentric bias, tending to anchor on the primary camera viewpoint and showing limited robustness in Level-2 visual perspective taking [12, 14].

We term this capability **Perspective-Conditioned Spatial Reasoning (PCSR)**. Given an observed scene, PCSR requires a model to update, re-anchor, and infer spatial relations with respect to a changed or hypothesized observer position, orientation, and viewpoint. Motivated by prior work on internal observer-conditioned spatial representation in navigation [2], we use *observer-conditioned spatial representation* to refer to an internal and manipulable scene representation indexed to the observer’s position, orientation, and viewpoint. In this paper, however, we do not attempt to directly observe such a representation. Instead, we operationalize it through tasks that require models to dynamically update, re-anchor, and recompute spatial relations under changed observer conditions.

Evaluating PCSR therefore requires reasoning under viewpoint change rather than merely recognizing spatial relations from a fixed camera view. However, existing benchmarks—notably including even recent omnidirectional frameworks [11]—do not directly target the core challenges of PCSR. To bridge this gap, we introduce PCSR-Bench, a benchmark designed to test whether models can recompute spatial relations under changed observer conditions. A central design goal of PCSR-Bench is to reduce the confound between incomplete observation and genuine reasoning failure.

PCSR-Bench is built on 360° panoramic images and 3D scene annotations, giving models near-complete scene coverage from a single observation and thereby reducing ambiguity caused by partial observation, while still requiring viewpoint-dependent inference [10]. This design helps separate failures of observation from reasoning. The benchmark is organized into tasks of increasing difficulty: **T0–T2** assess foundational perception under a static global view, whereas **T3–T7** target advanced PCSR. In this way, PCSR-Bench evaluates not only target localization but also whether models form dynamic, observer-conditioned spatial representation.

Systematic zero-shot evaluation on PCSR-Bench reveals a clear gap in current MLLMs’ spatial abilities. Models perform nontrivially

on foundational perception tasks, but degrade sharply on advanced PCSR tasks. This pattern recurs across advanced PCSR subtasks, indicating a shared systematic failures rather than a task-specific failure.

To probe the plasticity of this gap, we explore a reinforcement-learning-based intervention on PCSR-Bench. Recent work shows that RL can elicit stronger reasoning behavior in both language and multimodal models [17, 20]. Following this line, we use RL not to claim that the problem is solved, but to diagnose whether targeted training signals can partially improved recover it. Our results show that suitable reward design and task feedback improve performance on some advanced PCSR, but gains remain uneven and the broader gap between foundational perception and advanced PCSR persists. This suggests that perspective-conditioned spatial reasoning is not an automatic byproduct of general visual understanding, but a core capability requiring explicit modeling, targeted training, and dedicated evaluation.

In summary, we make three contributions. First, we **formally define PCSR** as the ability to update, re-anchor, and infer spatial relations under changing viewpoints, establishing it as a distinct core capability beyond fixed views. Second, we **introduce PCSR-Bench**, a 3D-grounded diagnostic benchmark built on omnidirectional observations and a structured task suite spanning foundational perception to advanced perspective-conditioned reasoning. Third, we use PCSR-Bench to provide a **diagnosis of current MLLMs** and to study the **partial plasticity of PCSR under RL-based intervention**, revealing both a stable perception–reasoning gap and limited but non-negligible recoverability.

## 2 Related Work

### 2.1 Visual Spatial Reasoning Benchmarks

Prior work has developed a progression of benchmarks evaluate spatial reasoning in MLLMs [25], ranging from controlled synthetic datasets to more explicit spatial diagnostics. Early datasets such as CLEVR [22], ShapeWorld [24], and NLVR [39] emphasized controlled compositional reasoning under synthetic settings, while NLVR2 [40] and GQA [1] moved to natural images with richer semantics and scene structure [21, 39, 40]. Later work made spatial reasoning more central: VSR focuses on fine-grained spatial-language understanding [30], SpatialVLM [4] and TopViewRS [26] study spatial VQA and map reasoning, and OSR-Bench [11], CoSpace [55], and Spatial457 [45] extend evaluation to omnidirectional, continuous-view, and 6D spatial settings.

These benchmarks substantially improve the evaluation of foundational spatial perception, including counting, relative distance estimation, directional judgment, and object-centric spatial reasoning [18, 19]. However, most remain tied to a *fixed observer perspective*. Even with panoramic or top-down inputs, models typically reason from the provided viewpoint rather than re-anchoring the observer under a hypothetical one [13, 16]. Thus, existing benchmarks are effective for measuring static spatial perception, but less suited for isolating perspective-conditioned spatial reasoning.

### 2.2 Perspective-Conditioned Reasoning

Recent work in embodied AI and multimodal reasoning has begun to touch on perspective-conditioned spatial reasoning (PCSR),

grounded on classic notions of mental rotation and viewpoint transformation [9, 37, 47]. Yet in most current benchmarks, PCSR is entangled with partial observability, sequential perception, and navigation or action planning. This confounding complexity makes it difficult to isolate failures specifically from viewpoint re-anchoring rather itself or from related factors such as missing observations or unstable scene representations [54]. While prior work on omnidirectional scene understanding has demonstrated that wide-field observations can mitigate blind spots [8, 53], such methods do not by themselves provide a principled diagnosis of a model’s ability to recompute spatial relations under shifting observer conditions. Motivated by this gap, our work aims to isolate PCSR in a controlled setting and enable a direct assessment of perspective-conditioned reasoning.

### 2.3 Enhancing Spatial Reasoning in MLLMs

While supervised fine-tuning has been the dominant paradigm for aligning MLLMs, it often favors surface-level pattern matching over robust multi-step inference [3, 33]. Recently, Reinforcement Learning (RL) has shown strong potential for eliciting deliberative reasoning in both language and multimodal models. By optimizing outcome- and process-level rewards [23, 41, 49], RL encourages extended chains of thought (CoT), yielding substantial gains in mathematical, coding, and visual reasoning tasks [6, 28, 46].

The extent to which RL can similarly improve perspective-conditioned spatial reasoning remains unclear. Unlike general visual QA, PCSR requires observer-conditioned spatial representation, performing coordinate transformations, and re-anchoring spatial relation under changed viewpoint. These mirror the core challenges of object-state tracking and spatial updating in embodied settings [42]. Recent benchmarks further suggest that current MLLMs struggle consistently when required to reason from non-camera or alternative viewpoints, exhibiting systematic egocentric bias and degraded performance across first-person and cross-view settings [5, 27, 44].

In this context, RL is not only a method of improving performance but also a diagnostic tool for assessing model plasticity. Thus, we employ reward-guided RL as a diagnostic intervention to test the recoverability of PCSR under controlled evaluation settings.

## 3 PCSR-Bench Construction

PCSR-Bench is formulated as a comprehensive evaluation framework, consisting of a scalable construction pipeline, a structured task suite dataset, and a rigorous evaluation protocol, as illustrated in Figure 2.

### 3.1 Task Suite

PCSR-Bench is organized into eight diagnostic tasks ( $T_0$  to  $T_7$ ), spanning foundational perception and advanced reasoning. As illustrated in Figure 1, it uses 2D/3D scene annotations to generate task instances on omnidirectional images, but evaluates models solely on raw panoramic inputs.

**Foundational perception tasks** ( $T_0$ – $T_2$ ) evaluate baseline visual grounding and spatial awareness directly from the 360° observation.  $T_0$  (**Object Counting**) tests object identification and

counting.  $T_1$  (**Relative Distance**) evaluates relative distance judgments between objects.  $T_2$  (**Relative Direction**) evaluates relative directional judgments between objects.

**Advanced perspective-conditioned reasoning tasks** ( $T_3$ – $T_7$ ) probe where models can update, re-anchor, and constrain spatial judgments under changed observer conditions (See Figure 1).  $T_3$  (**Compositional Chains**) tests multi-step relational composition, including transitive and compositional inference (e.g., inferring  $A$  relative to  $C$  given relations between  $A$ - $B$  and  $B$ - $C$ ).  $T_4$  (**Egocentric Rotation**) tests spatial updating under observer rotation.  $T_5$  (**Perspective Re-anchoring**) tests whether models can re-anchor spatial judgments to a new observer viewpoint, e.g., inferring left/right relations after relocating the observer to another position in the scene.  $T_6$  (**Ego-Distortion**) tests reasoning under omnidirectional projection distortion, e.g., when objects split by the 360° seam remain adjacent in 3D space.  $T_7$  (**Limited-FOV Visibility**) assesses occlusion and visibility judgments under restricted field-of-view (FoV) constraints.

### 3.2 Benchmark Construction

**Data Collection and Canonical 3D Scene Layout Construction.** We build PCSR-Bench upon **ReplicaPano** [10], a photorealistic indoor 360° panoramic dataset constructed on top of the high-fidelity Replica environments [38] and enriched rich scene annotations, including room layouts and oriented 3D object bounding boxes. However, these raw omnidirectional images and annotations are not yet directly suitable for reliable PCSR benchmark construction. Since omnidirectional images suffer from severe geometric distortion, inferring true 3D spatial relations purely from 2D visual cues is highly prone to errors. This 2D-3D perception gap hinders both the automatic generation of accurate QA pairs and reliable human verification [7, 43].

To address this issue, we transform the raw metadata of each panorama into a canonical 3D scene layout. This unified, structured representation explicitly organizes the room envelope (floor and ceiling), camera pose, object instances, geometric extents, semantic categories, and instance identities into a single operable space. This canonical layout serves as the operational substrate of our benchmark: it allows exact geometric computation, supports intuitive inspection through rendered 3D views, and provides a standardized foundation for subsequent QA generation.

**3D Geometry-Constrained QA Generation.** Unlike prior efforts [4] that attempt to lift Internet-scale 2D images into approximate 3D representations using expert vision models, our QA generation is strictly governed by explicit 3D mathematical and geometric relations (e.g., Euclidean distances, vector dot products, and rotation matrices) derived from the canonical layout. This design forces models to perform true spatial reasoning rather than relying on image-plane heuristics.

Specifically, for spatial reasoning tasks (e.g.,  $T_1$ ,  $T_3$ ,  $T_5$ ), we generate two evaluation formats: (1) Open-ended questions that test absolute localization and zero-shot reasoning without candidate hints, and (2) Multiple-Choice Questions (MCQ) featuring reasoning-critical distractors. Instead of sampling random negative options, we computationally design hard distractors based on exact 3D spatial relations. For instance, in distance comparison ( $T_1$ ), the distractor

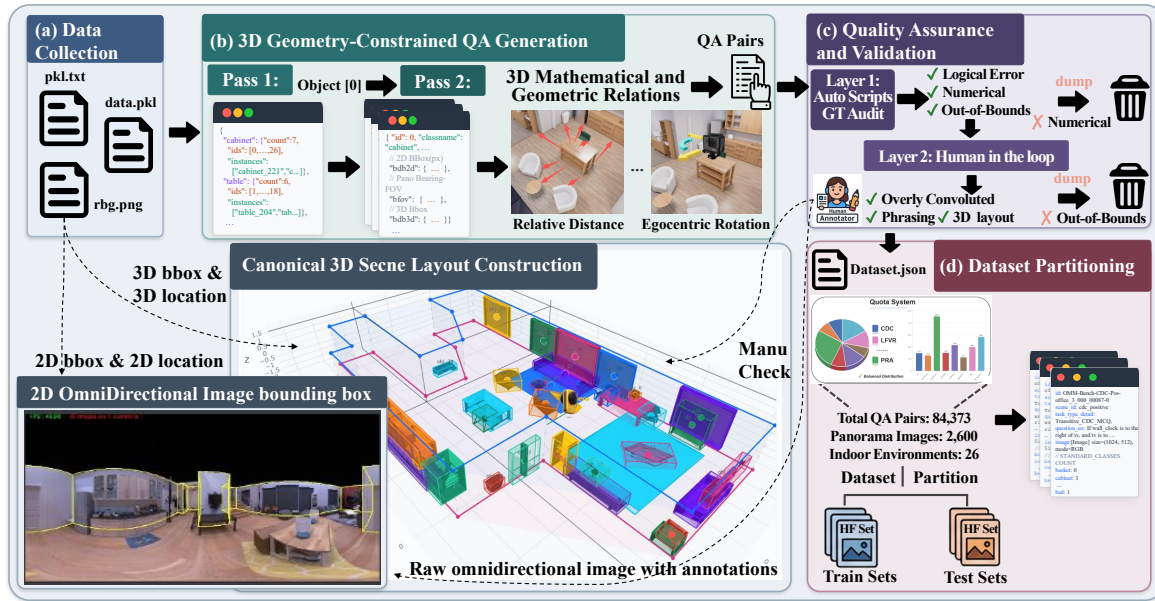


Figure 2: PCSR-Bench construction pipeline: ① a four-stage construction pipeline that programmatically generates diagnostic QA pairs from 3D ground truth; ② the resulting PCSR-Data; and ③ an evaluation protocol for assessing MLLMs on the benchmark.

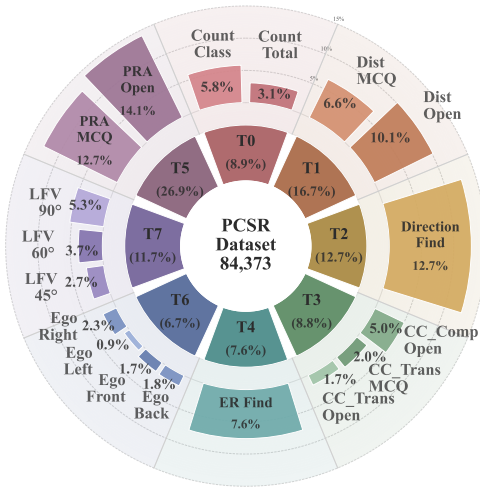


Figure 3: Task distribution of PCSR-Bench. The benchmark covers eight tasks, grouped into foundational perception (T0–T2) and advanced PCSR (T3–T7). The inner ring shows task proportions, and the outer rings show the breakdown by question format and advanced subtask type. MCQ denotes multiple-choice questions. CC, ER, PRA, Ego, and LfV denote Compositional Chains, Egocentric Rotation, Perspective Re-anchoring, Ego-Distortion, and Limited-FOV Visibility, respectively. Count, Dist, and Direction denote Object Counting, Relative Distance, and Relative Direction, respectively. For T3, CC-Trans and CC-Comp denote transitive and compositional inferences.

is explicitly set as the second-closest object; in compositional directional chains (T3), distractors are objects that satisfy only partial logical hops; and in counting tasks (T5), we deliberately include the 2D visible count as a distractor to penalize models that fail to account for 3D occlusion. This forces the model to execute precise numerical comparisons and complete logical deductions rather than relying on simple elimination. The implementation details of QA pair generation can be found in Appendix A.

**Quality Assurance and Validation.** To guarantee near-zero noise and absolute physical correctness, the generated data undergoes a rigorous two-stage quality assurance protocol. **First**, an **automatic integrity audit** verifies systematic and logical dimensions. This includes checking schema and value integrity, logic plausibility (e.g., ensuring answers strictly match predefined formats), and cross-modal referential integrity to guarantee perfect alignment between QA pairs and panoramic assets. A ground-truth-driven master audit then enforces a zero-tolerance policy, discarding any data exhibiting numerical or semantic deviations from the canonical 3D source. **Second**, a **human-in-the-loop validation** is conducted via task-wise stratified sampling. Beyond briefly checking for ambiguity, annotators rigorously evaluate the *naturalness* of the questions—ensuring the text is cognitively comprehensible and filtering out overly convoluted phrasing that could confuse both humans and multimodal models. Crucially, to assess *visual answerability*, annotators are provided solely with omnidirectional images (2.5D observations) without access to the 3D layout. The primary objective here is to validate the depth of our high-order reasoning tasks. Rather than merely observing the perception gap caused by spherical distortion or occlusion, this step ensures that our questions cannot be trivially solved via superficial 2.5D pattern matching. Instead, it verifies that successfully answering them strictly demands the formation of an internal, operable 3D cognition—directly aligning with our

core objective of evaluating dynamic, erspective-conditioned spatial reasoning.

**Dataset Partitioning.** Following the pipeline, PCSR-Bench ultimately yields 84,373 high-quality QA pairs, covering 26 distinct indoor scenes and associated with 2,600 high-resolution panoramas. To prevent MLLMs from exploiting visual memorization during training or fine-tuning, we adopt a strict image-level disjoint splitting strategy. The training and test sets are physically isolated at the panoramic image level, ensuring the test set authentically evaluates generalization and reasoning rather than data leakage.

## 4 Zero-Shot Evaluation on PCSR-Bench

### 4.1 Models and Setup

We evaluate 14 MLLMs spanning three capability tiers:

① Tier 1 ( $\geq 72\text{B}/\text{API}$ ): InternVL2.5-78B-Instruct, Qwen2.5-VL-72B, Qwen-VL-Max; ② Tier 2 (10B–40B): InternVL3.5-38B, Qwen3-VL-32B-Instruct, and Llama-3.2-11B-Vision-Instruct; ③ Tier 3 ( $< 10\text{B}$ ): InternVL2.5-8B, InternVL3.5-8B, Qwen2.5-VL-7B-Instruct, Qwen3-VL-8B, MiniCPM-V-2.5, LLaVA-v1.6-7B, LLaVA-OneVision-7B, Janus-Pro-7B. Compass (Ours) trains three GRPO variants on Qwen2.5-VL-7B-Instruct (see §5).

All models are evaluated on the PCSR-Bench test split (§3.2, 254 images, 9,697 samples), which is image-level disjoint from training data, ensuring evaluation on unseen scenes. For cross-model comparability, we use a unified zero-shot prompt (shown below) together with deterministic hard-greedy top-1 decoding. When necessary, architecture-compatible implementations are adopted only to ensure stable and valid generation, without changing the evaluation policy. Detailed are deferred to Appendix B.

*{Question}*

Output the thinking process in `<think>` and `</think>`,  
and the final answer (a single word or number) in  
`<answer>` and `</answer>` tags.

For models with native CoT capability (e.g., InternVL3.5 and Qwen3-VL), this template enables structured reasoning without additional system prompts.

### 4.2 Scoring Protocol

Exact-string matching can underestimate performance in zero-shot multimodal evaluation because semantically correct answers may vary in formatting, wording, and instance naming, especially under verbose CoT outputs [1, 31]. We therefore adopt a *Semantic-Aligned Evaluation Scorer*  $\mathcal{M}$  and define task-level accuracy as Eq. (1), using either its strict or relaxed variant depending on the reported metric.

$$\text{Acc} = \frac{1}{N} \sum_{i=1}^N \mathbb{I} \left[ \mathcal{M} \left( a_{\text{pred}}^{(i)}, a_{\text{gt}}^{(i)} \right) = \text{True} \right] \quad (1)$$

Before scoring, model outputs are standardized through light-weight answer extraction and normalization. We first remove the `<think>` content, then parse the `<answer>` block, and finally fall back to the first 200 characters when no explicit answer tag is present. We report both strict accuracy and relaxed accuracy: strict accuracy requires exact agreement after basic normalization, whereas relaxed accuracy applies a small set of ordered matching

heuristics, including intent canonicalization, domain synonym expansion, instance-to-class relaxation, and bounded substring matching. Full extraction and matching rules are provided in Appendix B.

## 4.3 Main Results and Analysis

Table 1 shows zero-shot top-1 relaxed acc on PCSR-Bench for 14 representative MLLMs in eight spatial-reasoning tasks. Models are grouped into three tiers by parameter scale or API access.

**Table 1: Zero-shot top-1 relaxed acc (%) on PCSR-Bench. Results are reported for 14 MLLMs across eight task categories grouped by cognitive type. Overall (all records) denotes pooled task-level accuracy computed over all answer records from the 14 models, rather than the mean of per-model scores. Bold = best in column; underline = second-best. †: proprietary API model. ‡: evaluated with CoT prompting.**

Model	T0	T1	T2	T3	T4	T5	T6	T7	Avg
<b>Tier 1: <math>\geq 70\text{B}</math> parameters or proprietary API</b>									
InternVL2.5-78B	<u>44.06</u>	29.45	<b>83.74</b>	26.45	15.49	<u>69.45</u>	9.42	21.99	<b>37.51</b>
Qwen-VL-Max <sup>†</sup>	39.91	<u>38.94</u>	<u>65.85</u>	<u>29.05</u>	<u>17.03</u>	69.60	<u>15.07</u>	21.03	<u>37.06</u>
Qwen2.5-VL-72B-Instruct	36.45	34.11	61.34	26.21	<b>17.36</b>	<b>71.32</b>	<b>17.50</b>	22.88	35.89
<b>Tier 2: 10–40B parameters</b>									
Qwen3-VL-32B-Instruct <sup>‡</sup>	34.72	38.44	58.45	28.93	15.82	41.08	<u>17.09</u>	20.49	31.88
InternVL3.5-38B	34.37	26.12	63.50	28.64	15.09	45.21	2.42	<u>22.53</u>	29.74
Llama-3.2-11B-Vision-Instruct <sup>‡</sup>	32.64	34.11	59.17	16.98	13.63	45.91	3.90	20.26	28.33
<b>Tier 3: <math>&lt; 10\text{B}</math> parameters</b>									
Qwen3-VL-8B-Instruct	38.29	<b>40.93</b>	46.52	<b>30.47</b>	16.46	66.48	4.44	17.95	32.70
MiniCPM-Llama3-V-2.5	<b>62.05</b>	32.45	36.86	20.18	6.24	54.33	12.79	22.03	30.86
InternVL2.5-8B	33.68	25.96	<u>75.70</u>	15.98	13.30	57.99	4.04	20.18	30.85
Qwen2.5-VL-7B-Instruct	37.02	23.29	63.78	19.23	13.38	57.29	3.77	<u>20.07</u>	29.73
deepseek-ai/Janus-Pro-7B	27.22	31.11	63.32	23.79	12.81	37.33	3.23	<u>23.30</u>	27.77
InternVL3.5-8B	25.72	16.64	54.20	20.77	13.06	63.13	2.02	15.65	26.40
llava-v1.6-vicuna-7b-hf <sup>‡</sup>	26.99	23.79	64.95	18.76	5.76	34.76	1.08	19.11	24.40
llava-onevision-qwen2-7b-ov-hf	20.76	29.12	8.85	20.53	13.38	59.55	3.10	<b>26.34</b>	22.70
<b>Overall (all records)</b>	35.28	30.32	57.59	23.28	13.49	42.98	7.13	20.99	28.88

### Scale helps, but architecture and generation matter more.

While larger models tend to perform better, we observe a clear decoupling between scale and performance on PCSR-Bench. Among Tier-1 models ( $\geq 70\text{B}$  or proprietary), InternVL2.5-78B achieves the highest average (37.51%), followed by Qwen-VL-Max (37.06%) and Qwen2.5-VL-72B (35.89%). Notably, the strongest Tier-3 model, Qwen3-VL-8B (32.70%), surpasses all Tier-2 models despite having 4–5 $\times$  fewer parameters, outperforming Qwen3-VL-32B (31.88%) and InternVL3.5-38B (29.74%). Similarly, within Tier-3, MiniCPM-V-2.5 (30.86%) and InternVL2.5-8B (30.85%) exceed all Tier-2 models except Qwen3-VL-32B. These cross-tier inversions indicate that improvements in model design and training can offset, or even surpass, gains from scale, making parameter count a weak predictor of PCSR performance.

**A persistent perception–reasoning gap.** Perception-oriented tasks are substantially easier than causal or compositional reasoning tasks across all models. T7 (LFV) achieves the highest pooled accuracy (57.59%), with InternVL2.5-78B reaching 83.74%. In contrast, T4 (ER) is the most challenging (7.13%; best: 17.50%), followed by T2 (Direction) at 13.49% (best: 17.36%). T3 (Causal Dependency Chain) requires careful interpretation due to strong internal disparity: the open-ended compositional subset achieves only 0.64%

relaxed accuracy, while the two transitive subsets reach 77.41% and 80.50% (see Appendix B for detailed subtask-level results). As a result, pooled T3 accuracy is 42.98%, but rises to 78.82% when considering only the transitive subsets—exceeding all other task categories (see Appendix C). These results indicate that current VLMs handle transitive chain inference far better than compositional spatial reasoning in open-ended settings.

**Instruction-following inconsistencies distort per-task profiles.** Two models exhibit anomalous per-task patterns that reflect output-format sensitivity rather than genuine capability differences. LLaVA-OneVision-7B, with an overall average of only 22.70%, scores 8.85% on T7 (LFV)—48.7 pp below the overall pooled T7 accuracy 57.59%—yet simultaneously records the best T5 (PRA) score across all 14 models (26.34%), indicating selective rather than uniform format failures. Conversely, MiniCPM-V-2.5 achieves the best T0 (Counting) score of any model (62.05%, some 27 pp above the T0 overall of 35.28%) while collapsing to 6.24% on T2 (Direction), the second-lowest value across all models. These cross-task disparities suggest that per-task performance is shaped not only by underlying reasoning ability, but also by task-specific factors that are not fully captured by a single task score. This observation motivates the robustness analysis in § 4.3.

**Sensitivity to scoring protocol.** To further probe the reliability of these measurements, we compare strict and relaxed accuracy across all models (see Appendix C for the full comparison). Relaxed scoring consistently yields higher accuracy than strict scoring across all 14 models. Averaged at the model level, strict accuracy is 24.08%, whereas relaxed accuracy rises to 28.88%, corresponding to a mean gain of 4.80 pp. The largest increase is observed for LLaVA-OneVision-7B (+20.59 pp), suggesting that exact-match evaluation can substantially undercount semantically correct predictions for some systems. At the same time, the gains for several other models remain comparatively modest, indicating that sensitivity to the scoring rule is uneven rather than universal.

While these zero-shot results highlight systematic failures, the following section explores the partial plasticity of these gaps through a diagnostic reinforcement learning pilot study.

## 5 RL Exploration on PCSR-Bench

To probe whether the observed reasoning gap is at least partially plastic, we conduct a reinforcement-learning-based intervention by fine-tune Qwen2.5-VL-7B-Instruct on the PCSR-Bench training split using GRPO [35]. This section serves as a diagnostic pilot study rather than a full solution to PCSR. Instead of numerically replacing the zero-shot results in § 4, it examines whether targeted reward design can improve perspective-conditioned spatial reasoning under a unified evaluation stack. Unless otherwise noted, all within-section comparisons are made under this controlled stack. Detailed training hyperparameters are deferred to Appendix D.

### 5.1 Training Setup

**Base model:** We use Qwen2.5-VL-7B-Instruct as the starting checkpoint. **Training data:** Training uses the PCSR-Bench training split, comprising 7,499 QA pairs spanning all eight task types (T0–T7) with a balanced mix of multiple-choice and open-ended questions. **Image processing:** Images are processed through the Qwen2.5-VL

dynamic-resolution pipeline with  $\text{max\_pixels} = 652,680$ . Since the native panoramic resolution is  $1024 \times 512$  (524,288 pixels), no down-scaling is required; each spatial dimension is rounded to a multiple of 28, yielding an effective processing resolution of  $1036 \times 504$ . **Training configuration:** All variants are trained for one epoch with maximum completion length 512 on  $8 \times \text{A800}$  (80GB) GPUs using DeepSpeed ZeRO Stage 2, FlashAttention-2, and bfloat16 precision. The per-device batch size is 1 with gradient accumulation over 4 steps (effective batch size 32). **Output format.** During RL training, we retain the same structured think-answer format used in evaluation, with reasoning enclosed in  $\langle \text{think} \rangle \dots \langle / \text{think} \rangle$  and the final prediction in  $\langle \text{answer} \rangle \dots \langle / \text{answer} \rangle$ .

### 5.2 360-R1 GRPO Objective and Reward Design

Following the 360-R1 framework [50], we employ Group Relative Policy Optimization (GRPO) [35, 51] as our reinforcement learning objective. Compared with conventional Proximal Policy Optimization (PPO) [36], which requires training an auxiliary value network, GRPO derives its advantage signal directly from group-level reward statistics, thereby reducing both computational overhead and implementation complexity.

Concretely, given a question  $q$ , the current policy  $\pi_{\text{old}}$  produces a group of  $G$  candidate responses  $\{o_1, \dots, o_G\}$ , each of which is assigned a scalar reward  $r_i$  by a reward model. These raw scores are then standardized within the group to yield zero-mean, unit-variance advantages:

$$\hat{r}_i = \frac{r_i - \text{mean}(\mathbf{r})}{\text{std}(\mathbf{r})}, \quad (2)$$

which serve as a constant advantage estimate across all token positions of the  $i$ -th response:

$$\hat{A}_{i,t} = \hat{r}_i. \quad (3)$$

Policy updates are carried out with a clipped surrogate objective to bound the magnitude of each step:

$$\mathcal{L}_{\text{clip}} = -\mathbb{E} \left[ \min \left( r_t \hat{A}_t, \text{clip}(r_t, 1-\epsilon, 1+\epsilon) \hat{A}_t \right) \right], \quad (4)$$

where the importance-sampling ratio is defined as  $r_t = \pi_{\theta}(o_t | q, o_{<t}) / \pi_{\text{old}}(o_t | q, o_{<t})$ . An additional KL penalty with respect to a reference policy  $\pi_{\text{ref}}$  is imposed to regularize training and prevent excessive policy drift:

$$\mathcal{L}_{\text{GRPO}}(\theta) = \mathcal{L}_{\text{clip}} + \beta \text{KL}(\pi_{\theta} \| \pi_{\text{ref}}). \quad (5)$$

By combining group-normalized advantages, clipped updates, and KL regularization, GRPO provides a lightweight yet effective optimization procedure that is particularly well-suited to our rule-based reward setting.

To optimize PCSR behavior, we instantiate the GRPO reward as a weighted combination of three components targeting answer correctness, structured generation compliance, and spatial reasoning fidelity:

$$r = \lambda_1 R_{\text{acc}} + \lambda_2 R_{\text{fint}} + \lambda_3 R_{\text{reason}} \quad (6)$$

The weights  $(\lambda_1, \lambda_2, \lambda_3)$  vary by training variant (Table 2); the main full-reward setting uses (0.60, 0.20, 0.20). Detailed reward definitions are provided in Appendix D.

**Table 2: RL variants and ablation settings under the unified evaluation stack. ID indicates the variant family: V1-a and V1-b are matched non-RL controls; V2–V5 vary reward composition and weight allocation; V6 and V7 further isolate the new reward implementations.  $\lambda_1:\lambda_2:\lambda_3$  denotes the weights of  $R_{\text{acc}}:R_{\text{fmt}}:R_{\text{reason}}$ .  $R_{\text{acc}}$  and  $R_{\text{fmt}}$  marked as *new/old* indicate the new/old implementations of the corresponding reward terms. Setting provides a compact description of each variant, and Purpose summarizes its role in the ablation design. H-Avg denotes the mean of T2, T4, and T5. Bold = best; underline = second-best. All eight variants are reported to avoid selection bias.**

Variant definition							Accuracy				
ID	$R_{\text{acc}}$	$R_{\text{fmt}}$	$R_{\text{reason}}$	Setting	$\lambda_1:\lambda_2:\lambda_3$	Purpose	Avg.	T2	T4	T5	H-Avg
<i>Matched non-RL controls</i>											
①-a	—	—	—	Base-style prompt control	—	Matched control (base-style prompt)	31.28	13.71	6.73	21.22	13.89
①-b	—	—	—	Train-style prompt control	—	Matched control (train-style prompt)	31.10	14.52	5.11	20.65	13.43
<i>Reward / weight ablations</i>											
②	new	new	—	Reason-free RL	0.50:0.50:0	Weight ablation (reason-free RL)	<u>63.06</u>	40.88	31.36	<b>37.06</b>	36.43
③	new	new	new	Balanced full reward	0.40:0.40:0.20	Weight ablation (balanced full reward)	34.80	15.09	27.59	27.07	23.25
④	new	new	new	Main full-reward variant (360-R1)	0.60:0.20:0.20	Main full-reward variant (360-R1)	60.06	<u>47.20</u>	<b>42.80</b>	30.87	<b>40.29</b>
⑤	new	new	—	No $R_{\text{reason}}$	0.75:0.25:0	Reason ablation (no $R_{\text{reason}}$ )	<b>65.27</b>	<b>50.85</b>	30.96	<u>35.02</u>	<u>38.94</u>
<i>Implementation ablations</i>											
⑥	new	old	new	Old $R_{\text{fmt}}$ implementation	0.60:0.20:0.20	Format-reward implementation ablation	29.56	14.19	24.09	20.65	19.64
⑦	old	new	new	Old $R_{\text{acc}}$ implementation	0.60:0.20:0.20	Accuracy-reward implementation ablation	41.34	15.57	<u>40.51</u>	25.37	27.15

All comparisons in this table are restricted to the unified § 5 setup, where controls and trained variants share the same inference backend and answer-extraction rules. Accordingly, these scores should be interpreted as internally controlled comparisons rather than direct numerical replacements of the earlier § 4 zero-shot result.

**Training Variants and Ablation Design** To disentangle the effects of reward composition, weight allocation, and reward implementation, we organize the experiments into two matched non-RL controls and six RL variants (Table 2). Variants ①-a and ①-b are matched non-RL controls evaluated under the same § 5 inference stack, serving to isolate gains from prompt formatting alone. Variants ②–⑤ vary reward composition and weight allocation, while Variants ⑥ and ⑦ isolate the new implementations of  $R_{\text{fmt}}$  and  $R_{\text{acc}}$  under the same full-reward setting. This design separates matched controls from RL variants, since the goal of § 5 is not direct comparison with § 4, but to examine which reward choices reshape PCSR behavior under a controlled evaluation stack. This design separates matched controls from RL variants as the goal of § 5 is not to make a direct compare with § 4, but rather to examine which reward choices reshape PCSR behavior under a controlled evaluation stack. For space efficiency, Table 2 reports only a compact cross-variant summary in the main text, while Appendix D contains detailed reward definitions, implementation settings, and full supporting materials—including complete metric breakdowns, implementation details, and additional qualitative examples, to avoid any impression of selective reporting.

### 5.3 Results and Analysis

This subsection consolidates our findings into three core conclusions. We demonstrate that the spatial reasoning deficits observed earlier are partially recoverable through RL, that this optimization improves internal logical consistency alongside aggregate scores, and that benchmark conclusions remain highly sensitive to the underlying evaluation protocol.

**Partial plasticity and the reward-design trade-off.** First, we establish that the systematic failures identified in § 4 are at least partially plastic. Under a unified evaluation stack, the matched non-RL controls (Variants ①-a and ①-b) achieve similar relaxed accuracies (~31.2%, Table 2), confirming that mere prompt rewriting cannot explain subsequent gains. Targeted RL substantially improves performance (up to 65.27% for Variant ⑤), proving that advanced PCSR behaviors can be recovered. However, this recovery is highly sensitive to both reward allocation and implementation. For instance, changing the reward weights (Variant ③ vs. ④★) or replacing the structured format reward with a binary check (Variant ⑥; see Appendix D for implementation details) drastically swings overall accuracy from 29.56% to 60.06%. Furthermore, the full-reward configuration (Variant ④★) reveals a critical task-dependent trade-off: while it does not maximize the global average, it achieves the highest performance (40.29%) on the most demanding reasoning-heavy

subset (T2/T4/T5). This indicates that the full reward is not a universal improver, but a targeted mechanism that sacrifices some performance on easier tasks to strengthen core PCSR reasoning.

**Beyond task scores: RL improves reasoning–answer consistency.** The benefits of reasoning-aware optimization extend beyond aggregate accuracy to the internal logical coherence of the model’s generation. As illustrated in the egocentric rotation case study (Figure 4), the baseline model not only predicts the wrong object but also exhibits a severe reasoning–answer mismatch: its intermediate text deduces that the *toilet* would be at the center, yet its final output is *window*. In contrast, our RL-optimized method maintains a coherent spatial update throughout its `<think>` trace and produces a final answer (*door*) that perfectly aligns with its intermediate reasoning. This qualitative evidence complements the benchmark results, confirming that the reward mechanism successfully penalizes disjointed logic and enforces strict consistency between the spatial reasoning chain and the final prediction on complex 90° viewpoint-conditioned transformations [32].

**Egocentric Rotation Case Study**

**Task: 90 Degrees Counter-Clockwise Rotation**  
**Question:** If you rotate 90 degrees counter-clockwise, what object would be at the center of your view?  
**Ground Truth: Door**

**✓ Ours**

`<think>` The image is a 360-degree equirectangular panoramic view, showing a bathroom with the following elements:  
 - A door on the left.  
 - A cabinet with a sink and a faucet in the center.  
 - A light fixture and mirror above the cabinet.  
 - A toilet and a window on the right.  
 - A hallway leading to another room in the background.  
 If you rotate 90 degrees counter-clockwise, the door on the left side of the image will be at the center of your view. `</think>`  
`<answer>` Door `</answer>`  
 — — green: correct object & position

Ours: coherent rotation reasoning

**✗ Baseline**

`<think>` The image is a 360-degree equirectangular panoramic view of a bathroom. The current view shows:  
 - A sink on the left.  
 - A toilet on the right and a mirror above the sink.  
 If we rotate 90 degrees counter-clockwise, the sink will be on the right, the mirror will be on the left, and the toilet will be in the center. The object at the center of the view would be the toilet. `</think>`  
`<answer>` window `</answer>`  
 — — green: correct | — yellow: imprecise (sink is center-left) | — red: wrong rotation logic & answer

Baseline: inconsistent reasoning

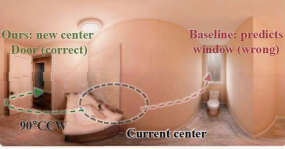


**Figure 4: Qualitative comparison of reasoning processes in an egocentric rotation example.** Given a 360° scene and the question of which object would move to the center after a 90° counter-clockwise rotation, our method correctly predicts *door*, while the baseline predicts *window*. The baseline also shows a reasoning–answer mismatch, whereas our method maintains a more consistent spatial update and a final answer that is consistent with its intermediate reasoning.

**Protocol sensitivity and methodological implications.** Finally, the discrepancy between the earlier Qwen2.5-VL-7B zero-shot results (§ 4) and the matched controls (§ 5) highlights a crucial methodological takeaway: PCSR evaluation is highly protocol-sensitive. For tasks involving panoramic visual inputs and long-form structured outputs, factors such as inference backend, visual preprocessing, generation budget, and answer parsing rules materially shape the final benchmark conclusions; detailed protocol differences are summarized in Appendix D. Consequently, the numerical results from § 4 & 5 cannot be rigidly aligned or directly swapped. Instead, these

findings emphasize that the evaluation strategy is an intrinsic part of the benchmark itself. While the spatial reasoning limitations of MLLMs are partially recoverable, robust benchmarking requires explicit protocol documentation and strictly matched inference settings for valid cross-variant comparisons.

## 6 Discussion

The findings of § 4–5 show that strong perceptual coverage does not guarantee robust spatial modeling [47, 48]. While panoramic inputs remove field-of-view limits, they expose a deeper bottleneck: current MLLMs struggle to simulate spatial changes. Failures in viewpoint transformation, re-anchoring, and multi-step composition suggest that models treat spatial relations as static 2D correlations rather than dynamic 3D structures.

Our RL analysis further reveals that this deficit is only partially plastic and comes with trade-offs. Strong reasoning rewards improve complex transformations but degrade basic perception, resembling a “reasoning tax” [34, 52]. The high sensitivity to reward design and the mismatch between intermediate reasoning and final outputs also highlight fragile spatial coherence, indicating reliance on shortcuts and the need for process-level supervision rather than outcome-based rewards.

Finally, the discrepancy between our zero-shot results and matched controls underscores a critical methodological issue: measured PCSR performance is highly protocol-sensitive. Seemingly minor choices in inference backends, visual preprocessing, and parsing heuristics can materially shift benchmark conclusions. This reinforces the need to explicitly report and control the entire evaluation stack when drawing conclusions about spatial reasoning abilities. A more detailed discussion of the study’s limitations, including the scope of panoramic projection types and the reliance on specific base models, is provided in Appendix D.

## 7 Conclusion

We introduced PCSR-Bench, a 360° benchmark to diagnose perspective-conditioned spatial reasoning in multimodal large language models from omnidirectional images. The benchmark reveals a clear gap: full-scene visual access improves coverage, but does not by itself yield robust viewpoint transformation, perspective re-anchoring, or composition spatial reasoning. Our RL-based diagnostic study further shows that this gap is partially plastic but not uniformly recoverable, yet the gains remain task-selective, reward-sensitive, and protocol-sensitive. Taken together, these findings do not overturn the benchmark diagnosis; rather, they show that PCSR is a genuine bottleneck with limited but non-negligible recoverability. Future work should therefore pursue stronger spatially grounded modeling, more effective reward design, and more carefully controlled evaluation protocols.

## References

- [1] Stanislaw Antol, Aishwarya Agrawal, Jiasen Lu, Margaret Mitchell, Dhruv Batra, C Lawrence Zitnick, and Devi Parikh. 2015. Vqa: Visual question answering. In *Proceedings of the IEEE international conference on computer vision*. 2425–2433.
- [2] Andrea Banino, Caswell Barry, Benigno Uria, Charles Blundell, Timothy Lillicrap, Piotr Mirowski, Alexander Pritzel, Martin J. Chadwick, Thomas Degris, Joseph Modayil, Greg Wayne, Hubert Soyer, Fabio Viola, Brian Zhang, Ross Goroshin, Neil Rabinowitz, Razvan Pascanu, Charlie Beattie, Stig Petersen, Amir Sadik, Stephen Gaffney, Helen King, Koray Kavukcuoglu, Demis Hassabis, Raia Hadsell, and Dharshan Kumaran. 2018. Vector-based navigation using grid-like representations in artificial agents. *Nature* 557, 7705 (2018), 429–433. doi:10.1038/s41586-018-0102-6
- [3] Collin Burns, Pavel Izmailov, Jan Hendrik Kirchner, Bowen Baker, Leo Gao, Leopold Aschenbrenner, Yining Chen, Adrien Ecoffet, Manas Joglekar, Jan Leike, et al. 2023. Weak-to-strong generalization: Eliciting strong capabilities with weak supervision. *arXiv preprint arXiv:2312.09390* (2023).
- [4] Boyuan Chen, Zhuo Xu, Sean Kirmani, Brian Ichter, Dorsa Sadigh, Leonidas Guibas, and Fei Xia. 2024. SpatialVLM: Endowing Vision-Language Models with Spatial Reasoning Capabilities. In *Proceedings of the IEEE/CVF Conference on Computer Vision and Pattern Recognition (CVPR)*. 14455–14465.
- [5] Sijie Cheng, Zhicheng Guo, Jingwen Wu, Kechen Fang, Peng Li, Huaping Liu, and Yang Liu. 2024. EgoThink: Evaluating First-Person Perspective Thinking Capability of Vision-Language Models. In *Proceedings of the IEEE/CVF Conference on Computer Vision and Pattern Recognition*. 14291–14302. doi:10.1109/CVPR52733.2024.01355
- [6] Paul F Christiano, Jan Leike, Tom Brown, Miljan Martic, Shane Legg, and Dario Amodei. 2017. Deep reinforcement learning from human preferences. *Advances in neural information processing systems* 30 (2017).
- [7] Benjamin Coors, Alexandru Paul Condurache, and Andreas Geiger. 2018. Spherenet: Learning spherical representations for detection and classification in omnidirectional images. In *Proceedings of the European conference on computer vision (ECCV)*. 518–533.
- [8] Thiago LT da Silveira and Claudio R Jung. 2023. Omnidirectional visual computing: Foundations, challenges, and applications. *Computers & Graphics* 113 (2023), 89–101.
- [9] Abhishek Das, Samyak Datta, Georgia Gkioxari, Stefan Lee, Devi Parikh, and Dhruv Batra. 2018. Embodied question answering. In *Proceedings of the IEEE/CVF Conference on Computer Vision and Pattern Recognition (CVPR)*. 1–10.
- [10] Yuan Dong, Chuan Fang, Liefeng Bo, Zilong Dong, and Ping Tan. 2024. PanoContext-Former: Panoramic total scene understanding with a transformer. In *Proceedings of the IEEE/CVF Conference on Computer Vision and Pattern Recognition (CVPR)*. 28087–28097.
- [11] Zihao Dongfang, Xu Zheng, Ziqiao Weng, Yuanhuiyi Lyu, Danda Pani Paudel, Luc Van Gool, Kailun Yang, and Xuming Hu. 2025. Are Multimodal Large Language Models Ready for Omnidirectional Spatial Reasoning? *arXiv preprint arXiv:2505.11907* (2025).
- [12] Qingying Gao, Yijiang Li, Haiyun Lyu, Haoran Sun, Dezhi Luo, and Hokin Deng. 2024. Vision language models see what you want but not what you see. *arXiv preprint arXiv:2410.00324* (2024).
- [13] Robert Geirhos, Jörn-Henrik Jacobsen, Claudio Michaelis, Richard Zemel, Wieland Brendel, Matthias Bethge, and Felix A Wichmann. 2020. Shortcut learning in deep neural networks. *Nature Machine Intelligence* 2, 11 (2020), 665–673.
- [14] Gracjan Góral, Alicja Ziarko, Piotr Miłoś, Michał Nauman, Maciej Wolczyk, and Michał Kosiński. 2025. Beyond Recognition: Evaluating Visual Perspective Taking in Vision Language Models. *arXiv preprint arXiv:2505.03821* (2025).
- [15] Gracjan Góral, Alicja Ziarko, Michał Nauman, and Maciej Wolczyk. 2024. Seeing through their eyes: Evaluating visual perspective taking in vision language models. *arXiv preprint arXiv:2409.12969* (2024).
- [16] Yash Goyal, Tejas Khot, Douglas Summers-Stay, Dhruv Batra, and Devi Parikh. 2017. Making the v in vqa matter: Elevating the role of image understanding in visual question answering. In *Proceedings of the IEEE conference on computer vision and pattern recognition*. 6904–6913.
- [17] Daya Guo, Dejian Yang, Haowei Zhang, Junxiao Song, Peiyi Wang, Qihao Zhu, Runxin Xu, Ruoyu Zhang, Shiyong Ma, Xiao Bi, et al. 2025. DeepSeek-R1 incentivizes reasoning in LLMs through reinforcement learning. *Nature* 645, 8081 (2025), 633–638.
- [18] Jiajie Guo, Qingpeng Zhu, Jin Zeng, Xiaolong Wu, Changyong He, and Weida Wang. 2025. SpatialGeo: Boosting Spatial Reasoning in Multimodal LLMs via Geometry-Semantics Fusion. In *2025 IEEE International Workshop on Multimedia Signal Processing (MMSp)*. IEEE, 24–29.
- [19] Jiacheng Hua, Yishu Yin, Yuhang Wu, Tai Wang, Yifei Huang, and Miao Liu. 2026. Unleashing Spatial Reasoning in Multimodal Large Language Models via Textual Representation Guided Reasoning. *arXiv preprint arXiv:2603.23404* (2026).
- [20] Wenxuan Huang, Bohan Jia, Zijie Zhai, Shaosheng Cao, Zheyu Ye, Fei Zhao, Zhe Xu, Yao Hu, and Shaohui Lin. 2025. Vision-r1: Incentivizing reasoning capability in multimodal large language models. *arXiv preprint arXiv:2503.06749* (2025).
- [21] Drew A Hudson and Christopher D Manning. 2019. Gqa: A new dataset for real-world visual reasoning and compositional question answering. In *Proceedings of the IEEE/CVF Conference on Computer Vision and Pattern Recognition (CVPR)*. 6700–6709.
- [22] Justin Johnson, Bharath Hariharan, Laurens van der Maaten, Li Fei-Fei, C Lawrence Zitnick, and Ross Girshick. 2017. CLEVR: A diagnostic dataset for compositional language and elementary visual reasoning. In *Proceedings of the IEEE/CVF Conference on Computer Vision and Pattern Recognition (CVPR)*. 2901–2910.
- [23] Daniel Kahneman. 2011. *Thinking, fast and slow*. macmillan.
- [24] Alexander Kuhnle and Ann Copestake. 2017. ShapeWorld: A New Test Methodology for Multimodal Language Understanding. *arXiv preprint arXiv:1704.04517* (2017).
- [25] Phillip Y Lee, Jihyeon Je, Chanho Park, Mikaela Angelina Uy, Leonidas Guibas, and Minhuyk Sung. 2025. Perspective-aware reasoning in vision-language models via mental imagery simulation. In *Proceedings of the IEEE/CVF International Conference on Computer Vision*. 9241–9251.
- [26] Chengzu Li, Caiqi Zhang, Han Zhou, Nigel Collier, Anna Korhonen, and Ivan Vulić. 2024. TopViewRS: Vision-Language Models as Top-View Spatial Reasoners. In *Proceedings of the 2024 Conference on Empirical Methods in Natural Language Processing (EMNLP)*. 1786–1807.
- [27] Dingming Li, Hongxing Li, Zixuan Wang, Yuchen Yan, Hang Zhang, Siqi Chen, Guiyang Hou, Shengpei Jiang, Wenqi Zhang, Yongliang Shen, et al. 2025. Viewspatial-bench: Evaluating multi-perspective spatial localization in vision-language models. *arXiv preprint arXiv:2505.21500* (2025).
- [28] Hunter Lightman, Vineet Kosaraju, Yuri Burda, Harrison Edwards, Bowen Baker, Teddy Lee, Jan Leike, John Schulman, Ilya Sutskever, and Karl Cobbe. 2023. Let’s verify step by step. In *The twelfth international conference on learning representations*.
- [29] Disheng Liu, Tuo Liang, Zhe Hu, Jierui Peng, Yiren Lu, Yi Xu, Yun Fu, and Yu Yin. 2025. Deconstructing Spatial Intelligence in Vision-Language Models. *Authorea Preprints* (2025).
- [30] Fangyu Liu, Guy Emerson, and Nigel Collier. 2023. Visual Spatial Reasoning. *Transactions of the Association for Computational Linguistics* 11 (2023), 635–651.
- [31] Yuan Liu, Haodong Duan, Yuanhan Zhang, Bo Li, Songyang Zhang, Wangbo Zhao, Yike Yuan, Jiaqi Wang, Conghui He, Ziwei Liu, et al. 2024. Mmbench: Is your multi-modal model an all-around player?. In *European conference on computer vision*. Springer, 216–233.
- [32] Tianyi Niu, Jaemin Cho, Elias Stengel-Esklin, and Mohit Bansal. 2026. RotBench: Evaluating Multi-modal Large Language Models on Identifying Image Rotation. In *Proceedings of the 19th Conference of the European Chapter of the Association for Computational Linguistics (Volume 1: Long Papers)*. 5546–5569.
- [33] Long Ouyang, Jeffrey Wu, Xu Jiang, Diogo Almeida, Carroll Wainwright, Pamela Mishkin, Chong Zhang, Sandhini Agarwal, Katarina Slama, Alex Ray, et al. 2022. Training language models to follow instructions with human feedback. *Advances in neural information processing systems* 35 (2022), 27730–27744.
- [34] Yiming Ren, Yujiu Yang, and Junjie Wang. 2026. Mitigating the Reasoning Tax in Vision-Language Fine-Tuning with Input-Adaptive Depth Aggregation. *arXiv:2603.26330* [cs.CV] <https://arxiv.org/abs/2603.26330>
- [35] Zhihong Shao, Peiyi Wang, Qihao Zhu, Runxin Xu, Junxiao Song, Xiao Bi, Haowei Zhang, Mingchuan Zhang, YK Li, Yang Wu, et al. 2024. DeepSeekMath: Pushing the Limits of Mathematical Reasoning in Open Language Models. *arXiv preprint arXiv:2402.03300* (2024). <https://arxiv.org/abs/2402.03300>
- [36] Zhihong Shao, Peiyi Wang, Qihao Zhu, Runxin Xu, Junxiao Song, Xiao Bi, Haowei Zhang, Mingchuan Zhang, Y. K. Li, Y. Wu, and Daya Guo. 2024. DeepSeekMath: Pushing the Limits of Mathematical Reasoning in Open Language Models. *arXiv:2402.03300* [cs.CL] <https://arxiv.org/abs/2402.03300>
- [37] Roger N Shepard and Jacqueline Metzler. 1971. Mental rotation of three-dimensional objects. *Science* 171, 3972 (1971), 701–703. doi:10.1126/science.171.3972.701
- [38] Julian Straub, Thomas Whelan, Lingni Ma, Yufan Chen, Erik Wijmans, Simon Green, Jakob J. Engel, Raul Mur-Artal, Carl Ren, Shobhit Verma, Anton Clarkson, Mingfei Yan, Brian Budge, Yajie Yan, Xiaqing Pan, June Yon, Yuyang Zou, Kimberly Leon, Nigel Carter, Jesus Briales, Tyler Gillingham, Elias Mueggler, Luis Pesqueira, Manolis Savva, Dhruv Batra, Hauke M. Strasdat, Renzo De Nardi, Michael Goesele, Steven Lovegrove, and Richard Newcombe. 2019. The Replica Dataset: A Digital Replica of Indoor Spaces. *arXiv:1906.05797* [cs.CV] <https://arxiv.org/abs/1906.05797>
- [39] Alane Suhr, Mike Lewis, James Yeh, and Yoav Artzi. 2017. A Corpus of Natural Language for Visual Reasoning. In *Proceedings of the 55th Annual Meeting of the Association for Computational Linguistics*. 217–223.
- [40] Alane Suhr, Stephanie Zhou, Ally Zhang, Iris Zhang, Huajun Bai, and Yoav Artzi. 2019. A Corpus for Reasoning about Natural Language Grounded in Photographs. In *Proceedings of the 57th Annual Meeting of the Association for Computational Linguistics*. 6418–6428.
- [41] Zhiqing Sun, Sheng Shen, Shengcao Cao, Haotian Liu, Chunyuan Li, Yikang Shen, Chuang Gan, Liangyan Gui, Yu-Xiong Wang, Yiming Yang, et al. 2024. Aligning large multimodal models with factually augmented rlhf. In *Findings of the Association for Computational Linguistics: ACL 2024*. 13088–13110.

- [42] Andrew Szot, Alexander Clegg, Eric Undersander, Erik Wijmans, Yili Zhao, John Turner, Noah Maestre, Mustafa Mukadam, Devendra Singh Chaplot, Oleksandr Maksymets, et al. 2021. Habitat 2.0: Training home assistants to rearrange their habitat. *Advances in neural information processing systems* 34 (2021), 251–266.
- [43] Keisuke Tateno, Nassir Navab, and Federico Tombari. 2018. Distortion-aware convolutional filters for dense prediction in panoramic images. In *Proceedings of the European Conference on Computer Vision (ECCV)*. 707–722.
- [44] Maijunxian Wang, Yijiang Li, Bingyang Wang, Tianwei Zhao, Ran Ji, Qingying Gao, Emmy Liu, Hokin Deng, and Dezhi Luo. 2026. Egocentric Bias in Vision-Language Models. *arXiv preprint arXiv:2602.15892* (2026).
- [45] Xingrui Wang, Wufei Ma, Tiezheng Zhang, Celso M. de Melo, Jieneng Chen, and Alan Yuille. 2025. Spatial457: A Diagnostic Benchmark for 6D Spatial Reasoning of Large Multimodal Models. In *Proceedings of the IEEE/CVF Conference on Computer Vision and Pattern Recognition (CVPR)*. 24669–24679.
- [46] Jason Wei, Xuezhi Wang, Dale Schuurmans, Maarten Bosma, Fei Xia, Ed Chi, Quoc V Le, Denny Zhou, et al. 2022. Chain-of-thought prompting elicits reasoning in large language models. *Advances in neural information processing systems* 35 (2022), 24824–24837.
- [47] Jihan Yang, Shusheng Yang, Anjali W Gupta, Rilyn Han, Li Fei-Fei, and Saining Xie. 2025. Thinking in space: How multimodal large language models see, remember, and recall spaces. In *Proceedings of the Computer Vision and Pattern Recognition Conference*. 10632–10643.
- [48] Baiqiao Yin, Qineng Wang, Pingyue Zhang, Jianshu Zhang, Kangrui Wang, Zihan Wang, Jieyu Zhang, Keshigeyan Chandrasegaran, Han Liu, Ranjay Krishna, et al. 2025. Spatial mental modeling from limited views. In *Structural Priors for Vision Workshop at ICCV'25*.
- [49] Tianyu Yu, Yuan Yao, Haoye Zhang, Taiwen He, Yuxuan Han, Gang Cui, Shiguang Hu, Weifeng Liu, et al. 2024. RLHF-V: Towards Trustworthy MLLMs via Behavior Alignment from Fine-grained Correctional Human Feedback. In *Proceedings of the IEEE/CVF Conference on Computer Vision and Pattern Recognition (CVPR)*. 12183–12193.
- [50] Kinshen Zhang, Zhen Ye, and Xu Zheng. 2025. Towards omnidirectional reasoning with 360-r1: A dataset, benchmark, and grpo-based method. *arXiv preprint arXiv:2505.14197* (2025).
- [51] Kinshen Zhang, Zhen Ye, and Xu Zheng. 2025. Towards Omnidirectional Reasoning with 360-R1: A Dataset, Benchmark, and GRPO-based Method. *arXiv preprint arXiv:2505.14197* (2025). <https://arxiv.org/abs/2505.14197>
- [52] Yiwei Zhang, Yixuan Li, and Song Gao. 2026. Do Vision Language Models Rotate in Mind? Evaluating Spatial Transformation Reasoning. <https://openreview.net/forum?id=up2LD7vVdW>
- [53] Yinda Zhang, Shuran Song, Ping Tan, and Jianxiong Xiao. 2014. Panocontext: A whole-room 3d context model for panoramic scene understanding. In *European conference on computer vision*. Springer, 668–686.
- [54] Rui Zhu, Xin Shen, Shuchen Wu, Chenxi Miao, Xin Yu, Yang Li, Weikang Li, Deguo Xia, and Jizhou Huang. 2026. Video-MSR: Benchmarking Multi-hop Spatial Reasoning Capabilities of MLLMs. *arXiv preprint arXiv:2601.09430* (2026).
- [55] Yiqi Zhu, Ziyue Wang, Can Zhang, Peng Li, and Yang Liu. 2025. CoSpace: Benchmarking Continuous Space Perception Ability for Vision-Language Models. In *Proceedings of the IEEE/CVF Conference on Computer Vision and Pattern Recognition (CVPR)*. 29569–29579.